ACS OMEGA

http://pubs.acs.org/journal/acsodf

Article

Role of Graphene Oxide in Bacterial Cellulose–Gelatin Hydrogels for Wound Dressing Applications

Muhammad Umar Aslam Khan, Goran M. Stojanović, Rozita Hassan,* T. Joseph Sahaya Anand,* Maryam Al-Ejji, and Anwarul Hasan*

Cite This: *ACS Omega* 2023, 8, 15909–15919

Read Online

ACCESS | Metrics & More | Article Recommendations

ABSTRACT: Biopolymer-based hydrogels have several advantages, including robust mechanical tunability, high biocompatibility, and excellent optical properties. These hydrogels can be ideal wound dressing materials and advantageous to repair and regenerate skin wounds. In this work, we prepared composite hydrogels by blending gelatin and graphene oxide-*functionalized* bacterial cellulose (GO-*f*-BC) with tetraethyl orthosilicate (TEOS). The hydrogels were characterized using Fourier-transform infrared spectroscopy (FTIR), scanning electron microscopy (SEM), atomic force microscope (AFM), and water contact angle analyses to explore functional groups and their interactions, surface morphology, and wetting behavior, respectively. The swelling, biodegradation, and water retention were tested to respond to the biofluid. Maximum swelling was exhibited by GBG-1 (0.01 mg GO amount) in all media (aqueous = 1902.83%, PBS = 1546.63%, and electrolyte = 1367.32%). All hydrogels were hemocompatible, as their hemolysis was less than 0.5%, and blood coagulation time decreased as the hydrogel concentration and GO amount increased under in vitro standard conditions. These hydrogels exhibited unusual antimicrobial activities against Gram-positive and Gram-negative bacterial strains. The cell viability and proliferation were increased with an increased GO amount, and maximum values were found for GBG-4 (0.04 mg GO amount) against fibroblast (3T3) cell lines. The mature and well-adhered cell morphology of 3T3 cells was found for all hydrogel samples. Based on all findings, these hydrogels would be a potential wound dressing skin material for wound healing applications.

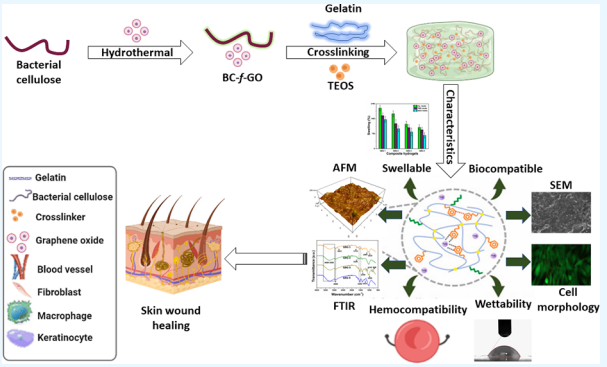

1. INTRODUCTION

The skin is a vital body organ that protects and functions as a barrier, shielding the body from its surroundings. Even though the skin has a significant capacity for self-regeneration, skin abnormalities larger than a specific diameter does not heal independently and require skin transplantation.[1,2] Additionally, the wound healing process is hindered in certain patients, resulting in chronic wounds that can lead to limb amputations or even death. Split- and full-thickness skin grafts, skin flaps, skin expansion procedures, and dermal replacements are among today's "gold standard" therapeutic options.[3,4] However, important issues linked with the available methods include donor site shortages and hypertrophic scars or keloids, resulting in severe functional and psychosocial issues. Tissue-engineered skin grafts, as a result, appear to be a viable option for overcoming these constraints. Skin tissue engineering is a rapidly expanding discipline to develop clinical skin substitutes.[5,6] A variety of wound dressing materials are employed as skin substitutes. It can be applied to the wound site to temporarily or permanently replace the functions of the skin, depending on the patient's requirements.

Various hydrogels, including natural and synthetic materials, have been fabricated similar to the extracellular matrix. Chemical or physical crosslinkings have been employed to produce hydrogels from synthetic and biopolymers.[7−10] Hydrogels are among the wound dressings designed to aid wound healing. They have emerged as some of the competitive wound dressing candidates. They are hydrophilic and biocompatible and have a three-dimensional porous structure similar to the extracellular matrix.[11,12] It has also piqued the interest of several researchers. The study has also increased hydrogels as wound dressings, particularly in the last decade. They have unique features that mimic the natural skin microenvironment compared to other biomaterials.[13,14] Hydrogels can also be utilized as injectable wound dressings.

Received: November 13, 2022
Accepted: March 1, 2023
Published: March 27, 2023

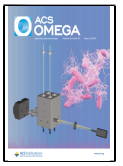

The addition of graphene oxide can strengthen these "multifunctional hydrogels", also known as "smart" hybrid hydrogels.

Natural polymers can fabricate hydrogels, and their mechanical strength can be enhanced by adding reinforcement materials or fillers. Bacterial cellulose (BC) is one of the most influential and available natural polymers with ultrafine fibers. *Acetobacter xylinum* is thought to be the most effective source of BC. Because its cellulose has β-1,4-glycosidic linkages between two glucose molecules,[15] its superior biomedical application could be employed in hydrogel composites for biomedical engineering. BC possesses many properties, including high Young's modulus, crystallinity, polymerization, surface area, and hydrophilicity.[16,17] A minor quantity of BC in gelatin-based hydrogels should be noted. When used under externally applied stresses, it can significantly improve tensile strength and dimensional stability.

Gelatin is a protein made by hydrolyzing collagen in an acid or alkaline solution. It is exceptionally biocompatible, biodegradable, non-immunogenic, and able for functional modification. On the other hand, gelatin is a low-cost, widely available natural polymer.[18] It is a processable and trendy material in biomedical engineering. Due to their transformability, several biomaterials can be designed in different shapes and forms. It is one of the potential materials among several biomaterials due to its promising results as a biomaterial in wound dressing, tissue engineering, and the release of therapeutic agents because of its unique and multifunctional nature.[19] Graphene oxide (GO) is among the well-known materials famous for their multifunctional properties. These include surface area and physicochemical and mechanical properties because of several available functional groups. It can easily be dispersed in polymeric solutions[20]—the improved properties of the hydrogel by adding GO into the hydrogel. For wound healing applications, GO-incorporated membranes have high mechanical strength and thermal stability and increased biological properties.[20,21]

This study offers optimization of GO amount and its role in the hydrogel system. BC was functionalized with different amount of GO by hydrothermal method and crosslinked with gelatin using TEOS to fabricate novel hydrogels to optimize GO amount and its role in different prepared formulations of hydrogels. The prepared formulations have never been reported before, according to best of our knowledge. The novel composition was used to develop stimuli-responsive hydrogels to treat skin wounds. Fourier transform infrared (FTIR), scanning electron microscopy (SEM), and water contact angles investigated the structural, morphological, mechanical, and wetting properties. The swelling was conducted in different media (aqueous, PBS, and NaCl). The biodegradation was observed in PBS media with a pH of 7.4 at 37 °C. The antibacterial activities were also performed using Gram (positive and negative) bacterial strains. The hemocompatibility was performed using fresh human blood—the cellular behavior of the hydrogels against fibroblast (3T3) cell lines using standard in vitro protocols. The fabricated hydrogel may be the potential biomaterial for wound healing applications.

2. MATERIALS AND METHODS

2.1. Materials. BC gelatin from bovine skin (G9382-500 g), GO (CAS no. 763713-1G), tetraethyl orthosilicate (CAS number: 78-10-4), PBS solution, HCl, absolute ethanol, and glacial acetic acid were provided by Sigma-Aldrich, Malaysia. Fibroblast (*3T3*) cell lines, α-MEM, were supplied by American Type Culture Collection (ATCC) and Hyclone Laboratories, respectively. L-Glutamine penicillin/streptomycin and fetal bovine serum were purchased from Thermo Fisher Scientific. Male albino mice were provided by the National Institutes of Health, Pakistan.

2.2. Methods. *2.2.1. Bacterial Culture and Production of Bacterial Cellulose.* BC was extracted in our previous study.[22] Briefly, the bacterial strains of *Gluconacetobacter xylinus* were isolated from rotten fruits. These bacterial strains were transferred into a 500 mL flask that contained 300 mL of Hestrin and Schramm medium. The flask was incubated for 48 h at 30 °C with continuous agitation, and the culture was used for the final BC synthesis. Then, 10 mL from the stock solution was transferred into a 250 mL flask to prepare a 10% v/v Hestrin and Schramm medium. The 250 mL flask was incubated for 7 days at 30 °C, and the formation of white gelatinous pellicle ware was observed on culture media. These white gelatinous pellicles indicate nanocellulose synthesis by BC. These white gelatinous pellicles were filtered for further purification of BC.

2.2.2. Purification of Bacterial Cellulose. The white gelatinous pellicles were harvested from the culture medium and treated with deionized water to wash medium components. The washed white gelatinous pellicles were shifted to a flask containing 0.1 M NaOH solution. The flask was incubated for 30 min at 80 °C until bacterial cells were separated from the polymeric matrix of BC. Then, the flask was removed and washed with deionized water until neutral pH. The purified BC was shifted to the Petri dish and freeze-dried until constant weight to have dried BC.

2.3. Fabrication of Hydrogels. The hydrothermal method was applied for BC and GO functionalization using different GO amounts (0.01, 0.02, 0.03, and 0.04 mg). Briefly, BC (2 g) was suspended in 50 mL of deionized water, and suspension of different GO amounts was stirred with BC polymeric suspension to have homogenized suspension. These homogenized suspensions with different GO amounts were shifted into a stainless-steel autoclave vessel separately and placed in an oven at 65 °C overnight to gelatin graphene oxide-*functionalized*-bacterial cellulose (GO-*f*-BC). The obtained polymeric composite was dispersed into 50 mL of deionized water and stirred with gelatin solution (0.3 g dissolved in 10 mL of deionized water) to get a homogenized solution for 1 h at 60 °C. Then, a hydrogel was obtained by adding TEOS ((240 μL) dissolved in 5 mL of ethanol) into a homogenized polymeric blended mixture and allowed to stir for 2 h at 60 °C. Then, potassium persulfate was added as an initiator and allowed to be stirred for another 3 h at 60 °C. After 3 h, the hydrogels were stored in glass vials for biological analysis. It was poured into Petri dishes and placed in the oven at 55 °C overnight to get the dried hydrogel. The codes to the hydrogels were assigned after different GO amounts (GBG-1 = 0.01 mg, GBG-2 = 0.02 mg, GBG-3 = 0.03 mg, and GBG-4 = 0.04 mg).

3. CHARACTERIZATIONS

FTIR was used to identify the functional group and cross-linkages in hydrogels in the wavelength range of 4000−600 cm^{-1}. The surface morphology of the hydrogel was determined by a scanning electron microscope (SEM). The SEM (JEOL-JSM 5410 LV) was used with an accelerated 10 kV voltage. Before analysis, the well-dried hydrogel films were gold-

https://doi.org/10.1021/acsomega.2c07279
ACS Omega 2023, 8, 15909−15919

sputtered for better electrical conductivity to determine the surface morphology. The surface roughness of the oven-dried hydrogels was conducted using an atomic force microscope (AFM) (Park Systems XE-100) to determine the surface topography of the hydrogels. We did not use the freeze-dried hydrogels due to their extreme porosity and rough surface behavior. The wetting behavior of the hydrogels was investigated by a water contact meter system (JY-82, Dingsheng, Chengde, China). After adding different cross-linking amounts, the wetting will help determine the hydrogels' change in hydrophilic and hydrophobic performance.

3.1. Swelling, Biodegradation, and Gel Fraction Analysis. The swelling analysis of oven-dried hydrogels was determined at 37 °C at different pHs to study the swelling characteristics of the prepared hydrogels, as we did not employ freeze-dried hydrogels due to their uneven surface roughness and morphology. The hydrogels were sliced in a square shape and weighed (50 mg) as the initial weight. These were dipped into different pH aqueous and PBS media. The excess surface water was wiped carefully using tissue paper, and the weight of the swelled hydrogel was recorded as the final weight after a suitable period. The swelling percentage was calculated by eq 1:

$$\text{Swelling}\ (\%) = \frac{W_f - W_i}{W_i} \times 100 \tag{1}$$

Similarly, the square-shaped hydrogels were weighed (50 mg) as the initial weight and were placed into PBS media with pH 7.4 at 37 °C. Then, the hydrogels were taken out after different time intervals to weigh as weight at "t" after removing extra surface media. The percentage weight loss was calculated by eq 2:

$$\text{Weight loss}\ (\%) = \frac{W_i - W_t}{W_i} \times 100 \tag{2}$$

The gel fraction of the hydrogels was determined in deionized water. The small pieces of the hydrogels were immersed in deionized water at room temperature for 12 h to remove unreacted reactants. The hydrogels were kept in methanol for 2 h and dried in an oven until constant weight. The gel fraction of the hydrogels was calculated by eq 3:

$$\text{Gel fraction}\ (\%) = \frac{M'}{M^\circ} \times 100 \tag{3}$$

where W_i is the initial weight, W_f is the final weight, W_t is the weight at "t" time, M' is the initial weight, and M° is the oven-dried weight.

3.2. In Vitro. *3.2.1. Antibacterial Assay.* The disc diffusion method was used to investigate the antibacterial activity of the prepared hydrogels. The antibacterial activity was determined by zone inhibition using Gram-positive (*Staphylococcus aureus* (*S. aureus*)) and Gram-negative (*Pseudomonas aeruginosa* (*P. aeruginosa*) and *Escherichia coli* (*E. coli*)) bacterial strains. We poured the molten agar nutrition into a Petri plate and waited for it to cool. A sterilized glass spreader was used to disperse the bacterial strains on the settled agar nutrient. The bacterial mediums were then spotted with 65 liters of hydrogels. For 12 h, these Petri dishes were incubated. Bacterial zone inhibition measurement was used to test antibacterial activity.

3.2.2. Hemocompatibility. Blood is an essential biofluid of our body as it directly interacts with any applied biomaterial and performs action accordingly. We have conducted the in vitro hemocompatibility of the composite hydrogels using fresh human blood. The trauma center kindly provided the fresh human blood, Public Hospital, Johor Bahru, Malaysia, and the assay was carried out by Ethics Committee approval. The Ethics Committee approval was obtained under UTM/2016/KHAIRUL NADWA/28-JAN/729-FEB-2016-JAN-2019. The in vitro hemocompatibility assay was conducted as reported in our previous study,[7] and hemolysis was calculated by eq 4:

$$\text{Hemolysis}\ (\%) = \frac{Abs_S - Abs_{NC}}{Abs_{PC} - Abs_{NC}} \times 100 \tag{4}$$

where Abs_S is the sample absorbance, Abs_{PC} is the positive control absorbance, and Abs_{NC} is the negative control absorbance.

Blood coagulation is one of the essential phenomena during injury or accident, as excessive bleeding most of the time causes death. In the meantime, we need a biomaterial that stops bleeding, protects it from the bacterial effect, and performs healing without scar formation. The bleeding stoppage is determined by blood coagulation, the time taken to coagulate blood as blood coagulation time. A citrated vacutainer tube was used to take the fresh blood and recalcified it by 5 μL of 0.05 M calcium chloride solution. Then, the blood was exposed to different concentrations (25−250 μg/mL) of composite hydrogels at 37 °C to observe blood flow.

3.2.3. Cell Viability and Proliferation. The cell viability and proliferation of hydrogels were determined using different dilutions (1.0 to 2.5 μg/mL). The fibroblast (3T3) cell lines were used to study the cell viability and proliferation after different time intervals (24, 48, and 72 h). The positive control was taken by a gelatin-coated (0.1%) well. All the well plates were incubated at 37 °C under standard in vitro conditions (90% humidity and 5% CO_2) for different time intervals (24, 48, and 72 h). The well plates were again incubated for 2 h using the neutral red (NR) method, according to Repetto et al.[23] PBS media washed the excess NR media, and optical density was measured at 540 nm using a microplate reader. The cell viability was calculated using eq 5:

$$\text{Cell viability}\ (\%) = \frac{OD_S}{OD_C} \times 100 \tag{5}$$

where OD_s is the sample optical density and OD_c is the control sample optical density.

3.2.4. Cell Adherence and Morphology. The cell adherence was evaluated using 3T3 cell lines at different intervals against all samples of the hydrogels. The fabricated hydrogels were washed with deionized water and dried in an oven for 24 h. These are again treated with ethanol to remove the additional GO flake over the oven-dried hydrogel surface to observe cell adherence and morphology of the 3T3 cell lines. After having a smooth surface, these hydrogels were sterilized under UV for 3−5 min. The cells were cultured on smooth hydrogel films for different times (24, 48, and 72 h) and treated with PBS to wash out non-adhered cells; however, the adhered cells were fixed by absolute ethanol. These hydrogel films were gold-sputtered, and SEM (JEOL-JSM-6480) was used to record the cellular behavior of the adhered 3T3 cells on hydrogel films.

3.3. Statistical Analysis. The statistical analysis of the research data was studied by statistical software (IBM, SPSS Statistics 21) except for the morphological and structural studies. The standard errors were presented in the figures as Y-error bars. With post hoc multiple comparisons, a two-way

https://doi.org/10.1021/acsomega.2c07279
ACS Omega 2023, 8, 15909−15919

ANOVA was used (*p < 0.05, **p < 0.01, and ***p < 0.001 size of sample n = 3).

4. RESULTS AND DISCUSSION

4.1. FTIR. The structural properties of hydrogels are observed in the FTIR spectra, as shown in Figure 1. The

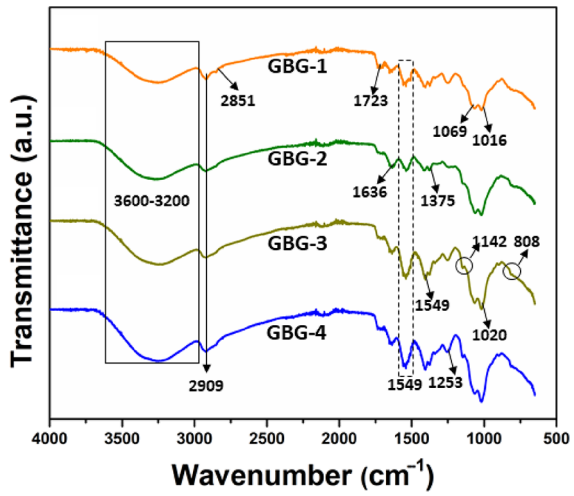

Figure 1. FTIR spectrum presenting the different functional groups of the hydrogels.

hydrogels (GBG-1, GBG-2, GBG-3, and GBG-4) confirm the corresponding peaks of the functional groups and their interaction. The broadband 3600−3200 is attributed to hydrogen bonding as both BC and gelatin contain −OH simultaneously. However, GO also contains −OH groups, and an increased intensity of the broadband was observed with an increased GO amount. The different broadband intensities are due to increasing crosslinking. The bands at 1228, 1053, and 1016 cm^{-1} are due to C−O stretching and pyranose, O−H bending vibration of the pyranose, and the pyranose ring, respectively.[24,25] These are characteristic peaks of the BC, and confirmation of these peaks confirms the presence of BC and gelatin. The absorption peaks at 2909 and 2851 cm^{-1} are due to $-CH_2$. The absorption peaks at 1723 and 1636 cm^{-1} are attributed to stretching vibrations of −C=C and −C=O; these absorption peaks are due to GO. Due to water molecules, the absorption peak at 1611 cm^{-1} is assigned to the OH functional group. The vibrational bands from 1187 to 912 cm^{-1} confirm the presence of gelatin and BC in hydrogels.[25] The vibration band between 1000 and 1100 cm^{-1} may be due to the TEOS crosslinker. The vibration peaks at 1069 and 1020 cm^{-1} result from the siloxane bond (Si−O−) and ensure the TEOS presence.[24,26] The hydrogels (GBG-1, GBG-2, GBG-3, and GBG-4) confirm the presence of all components (BC, gelatin, and GO) and TEOS crosslinks to the polymeric matrix.

4.2. Surface Morphology. The morphology of biomaterials is an essential characteristic, and SEM observed the surface morphology of the prepared hydrogels. Figure 2A shows a difference as hydrogels were dried at 55 °C in an oven overnight. However, Figure 2B presents a porous surface morphology as these hydrogel samples were freeze-dried. The rough surface was observed due to an increased GO amount that may crosslink with the polymeric chain. The increased micro/macro-islands were also observed due to an increased GO amount over the surface of hydrogels, as shown in Figure 2A. But it is also observed that this nano-island was shifted into micro/macro islands due to increased crosslinking.

It enhances the multifunctional surface properties of the hydrogels, helps cell adherence, and promotes cell proliferation, which enhances wound healing. The functional groups (−OH, $-COO^-$, $-CH_2OH$, etc.) may develop a multifunc-

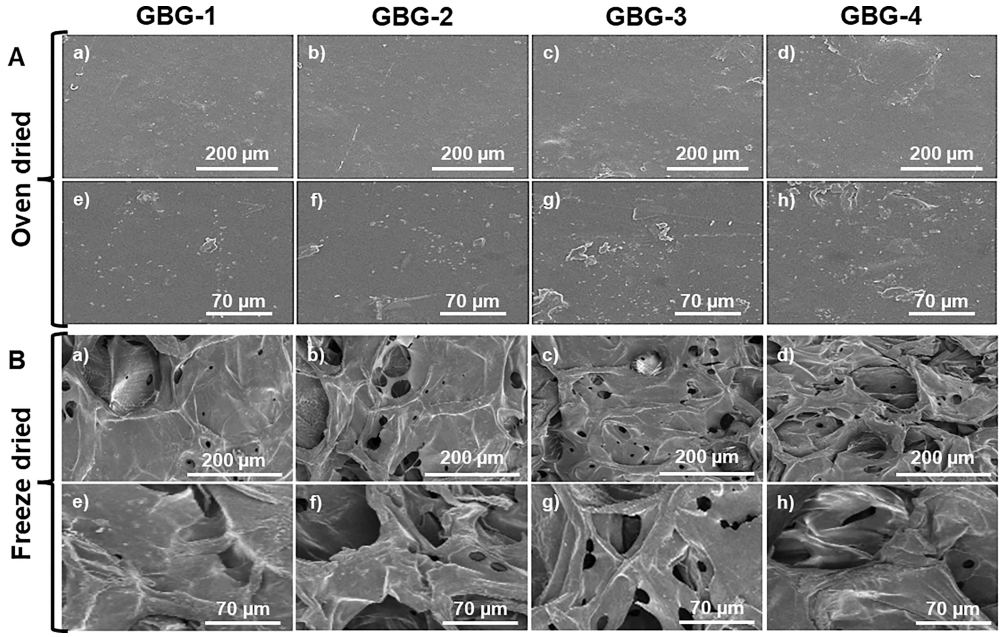

Figure 2. The surface morphology of hydrogels was observed at different scales (200 μm and 70 μm) to study their morphological behavior. A) The surface morphology of oven-dried hydrogels (a−h) have micro-/macro island/flakes were observed due to different incorporated amount of GO into the polymeric matrix of hydrogels, and the hydrogels have a similarity like a natural extracellular matrix. B) The porous surface morphology of freeze-dried hydrogels (a−h) was studied to investigate different pore size. The surface morphology can be changed by changing fabrication method and the incorporated GO may impart multifunctional behavior in the hydrogels.

https://doi.org/10.1021/acsomega.2c07279
ACS Omega 2023, 8, 15909−15919

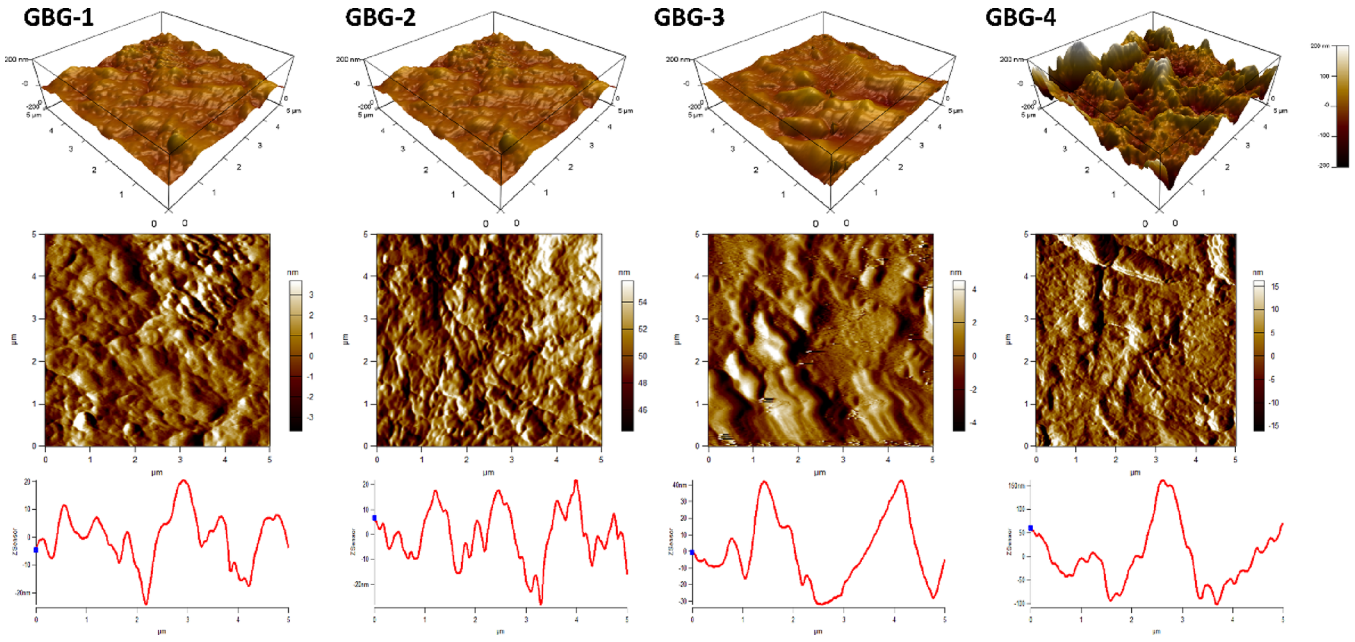

Figure 3. Surface roughness of the hydrogels observed by AFM analysis.

tional and friendly microenvironment of the hydrogels to promote biological activities for wound healing.[27,28] However, porous hydrogels also have multifunctional characteristics as porous hydrogels offer cell adherence, migration, and exchange of waste, gases, and nutrients, which are attributes of the ideal wound dressing materials.[29] The freeze-dried hydrogels have porous morphologies, and an increased GO amount causes an increased porosity from GBG-1 to GBG-4, as shown in Figure 2B. From the morphological analysis of the hydrogels, it can be concluded that changing the drying method can change the morphological behavior of the hydrogels. The increased GO amount enhances the multifunctionalities and increases the structural integrity. Hence, the SEM morphology confirms that GO has been successfully incorporated into the polymeric matrix of well-crosslinked hydrogels, and increasing the GO amount causes uneven or rough surfaces of hydrogels.

4.3. Surface Roughness. The surface topography of oven-dried hydrogel samples was analyzed by AFM (Figure 3). A rough and uneven surface was observed due to various GO amounts integrated into the composite's crosslinked composite network. The results noted that increasing the GO content causes growth in the high surface area and roughness of hydrogels. The increased surface area has increased an active or binding site that promotes cell adhesion and proliferation.[3,14] GBG-4 shows the most excellent surface area and roughness values, and GBG-1 composite samples displayed minimal surface roughness (Figure 3 and Table 1). In a biological environment, surface roughness is crucial for cell adherence to a hydrogel that will further increase, which helps wound healing. Compared to smooth surfaces, rough surfaces frequently have more significant friction coefficients and faster wear rates. Surface roughness also promotes the beginning of biodegradation and can help predict the mechanical attributes of hydrogels. The increased surface roughness causes more surface area, and only a substantial GO amount is suitable in hydrogels; otherwise, it may change the hydrogel properties. The mechanical and physiological interactions can be estimated more accurately at surfaces such as contact stiffness and static friction.[14,30] The hydrogel with a rough surface facilitates cell adherence, leading to cell viability and proliferation. The increased GO amount caused more surface roughness and surface area, which may enhance the biological behavior of the hydrogels. Hence, only a tiny GO amount is suitable in hydrogels; otherwise, too high a GO amount may alter the properties of hydrogels that may not be helpful in wound healing applications.

Table 1. Summary of the Obtained AFM Data and Increased RMS Values with an Increased TEOS Amount

	sample code			
AFM data	GBG-1	GBG-2	GBG-3	GBG-4
RMS (nm)	14.567	16.995	18.085	55.732
skewness	0.325	0.218	0.158	0.329
kurtosis	0.795	−0.0466	0.352	1.75
surface area (μm^2)	17.2	23.3	28.3	32.5
area percent (%)	0.7757	1.21	1.321	10.09

4.4. Wetting Analysis. The hydrophobicity and hydrophilicity of biomaterials—known as wettability—are crucial for biomedical engineering and are influenced by the water contact angle. While talking about wound healing, the hydrogels have directly interacted with the biofluids. The biofluids primarily consist of water, blood cells, and other essential minerals and electrolytes. It was observed that increasing crosslinking shifted the wetting behavior from hydrophilicity to less hydrophilic behavior.[31,32] It is also worth mentioning that the GO-*f*-BC has presented maximum hydrophilicity. The GBG-1 has the highest water contact angle at room temperature (Figure 4a,b) after different time intervals (5 and 10 s). It could be attributed to the availability of hydrophilic functional groups in GO (as mentioned in FTIR), which are increased with an increased GO amount. As shown, an increased water contact time switched the wetting behavior from hydrophobicity to hydrophilicity. It could be due to the interaction of different hydrophilic functional groups with water, which enhances hydrogen-bonding formation.

https://doi.org/10.1021/acsomega.2c07279
ACS Omega 2023, 8, 15909−15919

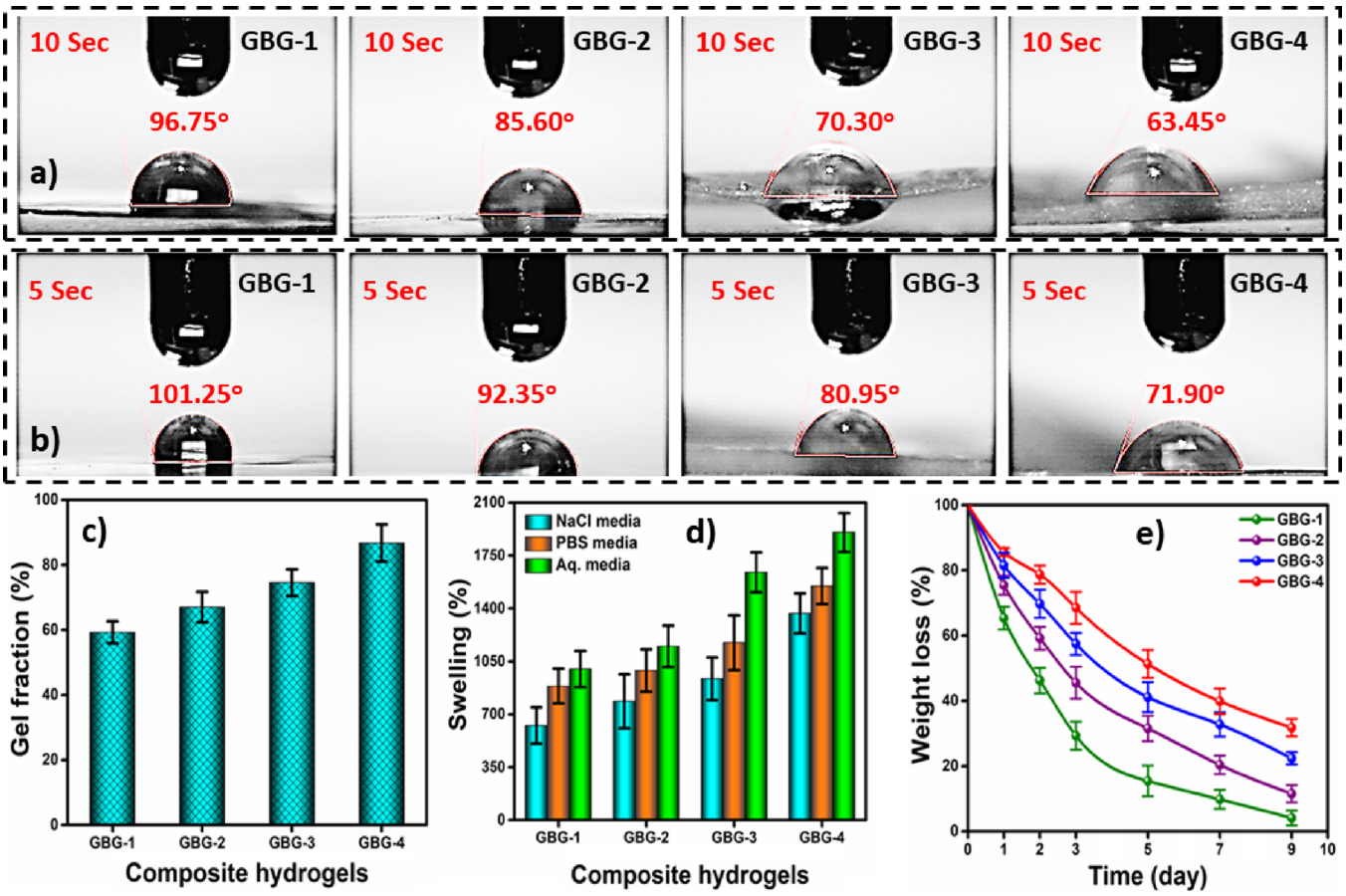

Figure 4. The wetting of hydrogels, gel fraction, and swelling have been presented to determine their behavior while interacting with biofluids. The wetting behavior was conducted to determine hydrophilic and hydrophobic behavior at room temperature (a, b), gel fraction that exhibited at room temperature (c), and swelling of the hydrogel in different media (aqueous, PBS, and NaCl media) at 37 °C (d) and (e) biodegradation of the hydrogels in PBS media at 37 °C.

Similarly, the increasing crosslinking degree shifted the hydrophobicity toward the hydrophilicity nature of hydrogels, which may be due to the tight or close packing of the polymeric matrix.[33,34] The increased water contact angle may be due to decreased hydrophilic functional groups during crosslinking. The increasing crosslinking may engage the hydrophilic function groups and increase the hydrogels' structural integrity. Hence, it was found that these hydrogels have successful crosslinking of GO-*f*-BC and gelatin.

4.5. Gel Fraction. The gel fraction of any biomaterial is the measurement of gel formation from the polymers. It is due to the physicochemical interaction between gelatin and GO-*f*-BC via different available functional groups. The gel fraction of the hydrogel is shown in Figure 4c. It was observed that increased crosslinking of gelatin and GO-*f*-BC had increased the gel fraction of the hydrogels from GBG-1 to GBG-4. The fluidity of the hydrogels decreases by increased crosslinking and other weak physical interactions like electrostatic, hydrogen-bonding, and $\pi-\pi$ interactions. These physicochemical interactions play an important role in gel formation. Rapid gel formation is essential to stop bleeding during trauma or accident by absorbing wound exudate.[35,36] The gel formation is also determined by the crosslinking degree. It was observed that increasing GO amount has shifted the low gel fraction (GBG-1) to high gel fraction (GBG-4). As a result, the growing gel fraction was observed due to an increased amount of GO, confirming the successful crosslinking of hydrogels due to TEOS crosslinking and a high amount of GO.

4.6. Swelling and Biodegradation Behavior. The swelling is also a critical behavior of the biomaterials, and on interacting with biofluid, the materials exhibit different behaviors depending on the environment and other parameters. The polymeric material swells after absorbing the biofluid when they contact the biofluids and the swelling. The swelling of hydrogels was performed in different media (such as aqueous, PBS, and NaCl media) at 37 °C to determine their swelling behavior while in contact with biofluid. Under the same temperature conditions, it was discovered that the relative swelling behavior was greatest in aqueous (deionized water), intermediate in PBS media, and least in NaCl media, as shown in Figure 4d. A decreased swelling was observed by increasing crosslinking. The maximum swelling in aqueous media was due to the hydrophilic behavior of the hydrogel that fell from GBG-1 to GBG-4. The comparatively less swelling of the hydrogel in PBS media was due to the ionic concentration of the available minerals in PBS media. However, the slightest swelling in hydrogels in NaCl (electrolyte media) is due to ion concentrations of Na^+ and Cl^- ions. The hydrogels may not allow the diffusion of the electrolyte media into the polymeric matrix of the composite polymers. Therefore, these hydrogels will swell quickly by absorbing wound exudate to hydrate the wound to regulate temperature.[37]

https://doi.org/10.1021/acsomega.2c07279
ACS Omega 2023, 8, 15909−15919

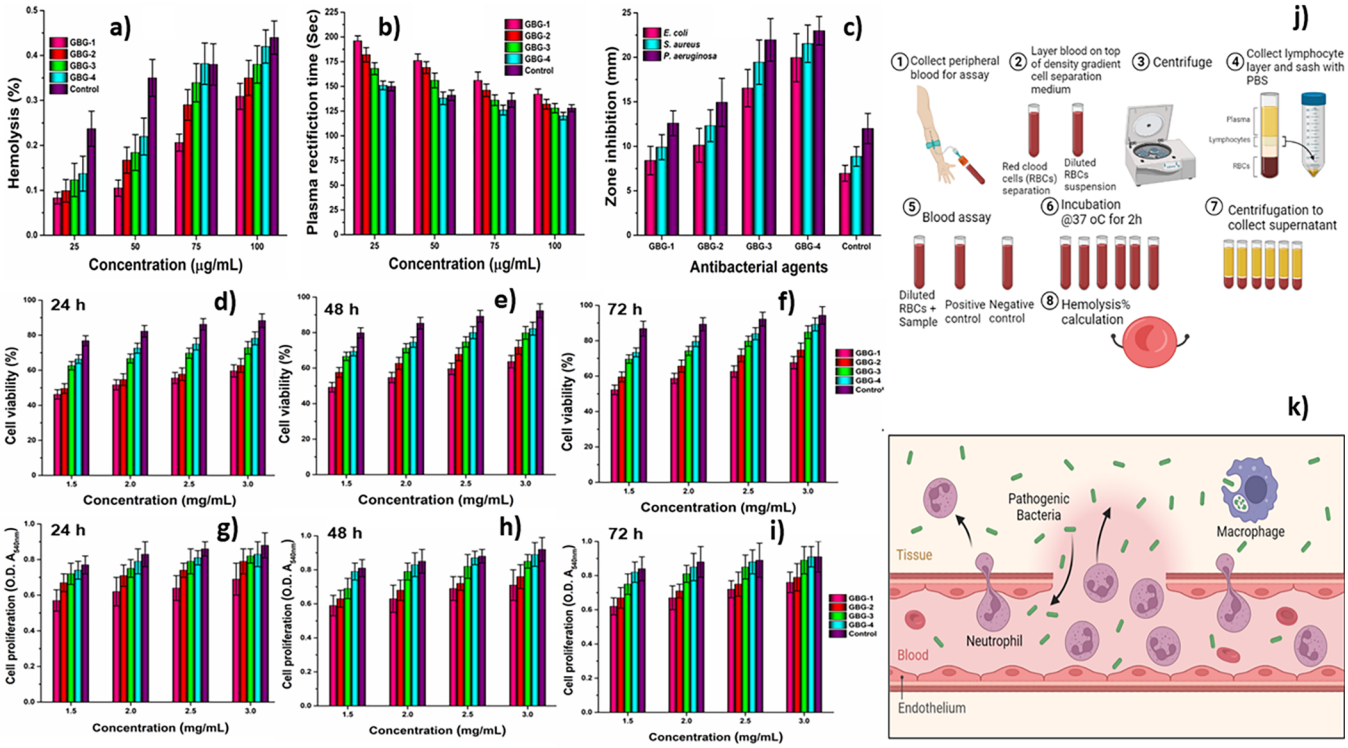

Figure 5. In vitro hemocompatibility and antibacterial activities of hydrogels. (a) Hemolysis characteristics, (b) blood clotting time, and (c) antibacterial activities of hydrogels against severe skin infection-causing Gram (positive and negative) pathogens. The cell viability (d−f) of hydrogels was determined after different time intervals (d = 24, e = 48, and f = 72 h) and cell proliferation (g−i) after different time intervals (g = 24, h = 48, and i = 72 h). It was found that contact time and increased crosslinking have resulted in increased cell viability and proliferation under in vitro standard conditions. (j) Hemocompatibility procedure and (k) antibacterial mechanism.

The swelling and biodegradation are correlated, which are very important for wound healing applications. The controlled biodegradation rate provides desired nutrient delivery and a friendly microenvironment that will be helpful for cell adherence to promote wound healing.[38] Figure 4e illustrates our investigation into biodegradation using various crosslinking rates and durations. It was found that increasing time and crosslinking caused delayed and continuous degradation. Of all the hydrogel samples, GBG-4 degrades the least, while GBG-1 degrades the most. The degradation trend was shifted from less to the maximum with the least crosslinking and maximum contact time with PBS media at 37 °C, as shown in Figure 4e. Hence, the different swelling behaviors in various media and biodegradation of hydrogels have confirmed the successful crosslinking. It also confirmed the swelling behavior against biofluid and biodegradation in stimulated blood fluid.

4.7. In Vitro Assays. *4.7.1. Hemocompatibility.* Hemocompatibility is one of the most critical aspects limiting biomaterials' clinical use and when the biomaterials come into direct contact with blood. Blood is a complex biofluid comprised of 1% leukocytes and platelets, 44% erythrocytes, and 55% plasma. Thus, adverse interactions between newly developed materials and blood should be extensively analyzed to prevent the activation and destruction of blood components.[39] The initial protein adsorption layer on the biomaterial surface might cause undesirable effects, including coagulation activation via the signal transduction mechanism. The inflammation may be caused by stimulating leukocytes, platelet adherence, and activity.[40] The volume of blood cells may decrease as a result, and a thrombus may develop. In vitro hemocompatibility of the composite hydrogel was performed against fresh human blood. The hemolysis assay has also been studied to analyze its hemocompatibility against different concentrations of hydrogels (25, 50, 75, and 100 μg/mL), as in Figure 5a. Since the hemolysis rate of all hydrogels is less than 0.5%, all the hydrogels are hemocompatible. The nominal hemolysis rate could be due to the cell rupturing with an interaction with sharp GO edges.[1,41] The blood coagulation properties of the hydrogels were also conducted, as shown in Figure 5b. It was observed that all hydrogels have different blood clotting properties. It was found that increasing crosslinking density of the hydrogels caused quick blood clotting, and coagulation time was found to be the best for GBG-4 among all the hydrogels. Only a substantial GO amount is suitable to be incorporated into the polymeric matrix; otherwise, it may harm the blood cells, but we are applying it for tropical wound healing.[42] Hence, the hydrogels are hemocompatible in nature and could be the best wound dressing material in wound healing for skin tissue engineering.

4.7.2. Antibacterial Activities. As shown in Figure 5c, the hydrogels have antibacterial activity against Gram (positive and negative) bacterial strains. Zone inhibition was used to test the antibacterial properties of the hydrogels. It was found that these hydrogels have an increasing trend of antibacterial activity from GBG-1 to GBG-4. It is also observed that these hydrogels have the least antibacterial against *E. coli* and the maximum toward *P. aeruginosa*. This is because the hydrogels are multifunctional due to synergistic effect of GO, BC, and gelatin, which are being crosslinked by TEOS. These functionalities can be due to the interactive phenomena of gelatin/BC with the bacterial membrane that is consisted of phospholipids and lipopolysaccharides. The polymeric material

https://doi.org/10.1021/acsomega.2c07279
ACS Omega 2023, 8, 15909−15919

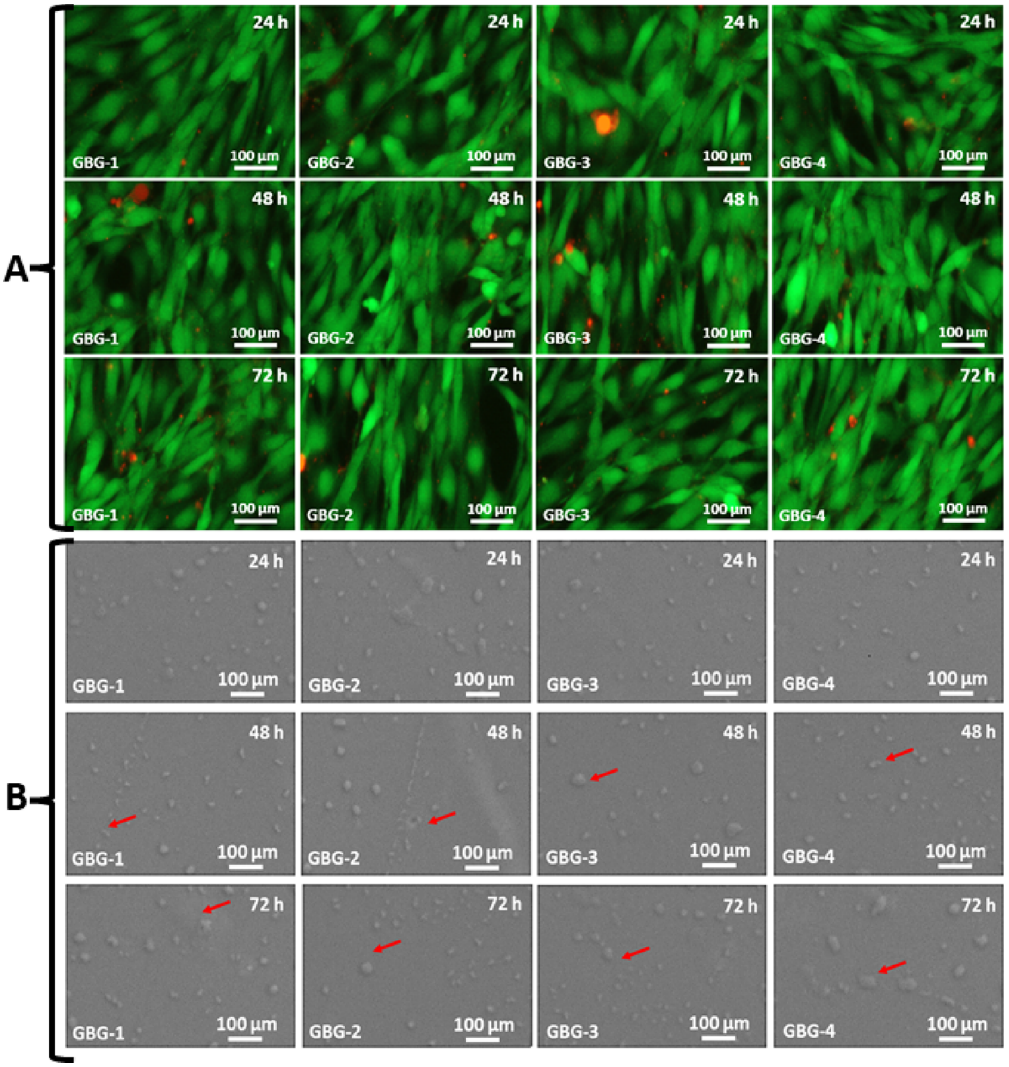

Figure 6. Cellular behavior of fibroblast cell lines against hydrogels. (a) Cell morphology against hydrogels after different times (24, 48, and 72 h) to determine the cellular behavior. (b) Cell adherence of 3T3 cell lines over hydrogels at different times (24, 48, and 72 h) to determine the adherence behavior. It was found that increased contact time increased cell population and cell adherence under in vitro standard conditions.

may induce charges into the bacterial membrane to inhibit bacterial growth. The second factor, the polymeric part of the hydrogel, may be bonding with bacterial DNA to prevent further transcription and translation.[43,44] The polymeric part of these hydrogels also has intermolecular forces and may penetrate the bacterial cell to control the transformation of the bacterial DNA. The third factor is that the sharp edges of GO may rupture the bacterial membranes to destroy the bacterial structure and, ultimately, no further growth. However, the overall antibacterial activity of these hydrogels due to their synergistic effect may result in the electrostatic interaction with the bacterial membrane. Therefore, wound healing can be accelerated by the enhanced synergistic effect of the multifunctional materials to kill bacterial pathogens.[45] These multifunctional hydrogels then develop a protective antibacterial shield that lasts until they biodegrade completely. The hemocompatibility and antibacterial process of hydrogels are shown in Figure 5d,e. Hence, the presented hydrogels might be promising wound dressing materials for fast wound healing applications.

4.7.3. Cell Viability and Proliferation. Cell viability and proliferation are critical for any biomaterial, and the hydrogel presents an additional hurdle for wound dressing applications. The biocompatible behavior of these hydrogels against 3T3 cell lines is shown in Figure 6. It was observed that the cell viability was increased by increasing the time, concentration, and crosslinking of hydrogels.[46] It was observed that an increasing GO amount in hydrogels increased the multifunctional behavior of hydrogels. The multifunctional behavior provides more active binding sites with an increased surface area that promotes cell adherence to enhance cell viability and proliferation, as shown in Figure 6d–f. It was also noted that increased hydrogel concentration (1.5 to 3 mg/mL) also facilitated cell viability and proliferation as saturated or more concentrated samples provided more binding and active sites. The increasing contact time (24 to 72 h) with hydrogels also favored cell viability and proliferation as cells get more time to adhere, facilitating cellular protein production. The cell viability has been conducted at different time intervals to determine the biocompatible behavior of hydrogels concerning time, as shown in Figure 6g–i. Cell proliferation has a similar behavior as it was observed for cell viability. The cell viability and proliferation can be due to the increased structural integrity and controlled multifunctionality of hydrogels by

https://doi.org/10.1021/acsomega.2c07279
ACS Omega 2023, 8, 15909−15919

increasing crosslinking, as GO also provides an additional binding site.[47,48] Hence, the cell viability and proliferation assay exhibits that these hydrogels are biocompatible and shall be potential wound dressing materials for skin tissue engineering.

4.7.4. Cell Morphology and Adherence. Hydrogels have a significant role in the availability of binding sites for cell adherence. The hydrogels fabricated from cellulose have fewer potential binding sites and poor cell adherence. However, by adding GO to promote cell adhesion, the functionality of hydrogels has been improved. The additional binding sites substantially impact the cell behavior and shape. In contrast to hydrogels lacking accessible binding sites, because of GO, the multifunctional behavior of hydrogels that allow binding has a distinctive cytoskeletal structure.[49] The adhered cells to hydrogels exhibit a spread or stretched shape and high actin-stressing fiber content and present a proper cell morphology, as shown in Figure 6a,b. GBG-4 hydrogels observed maximum cell adherence with a stretched morphology of 3T3 cell lines due to maximum GO incorporation. The cytoskeletal behavior of the cell can also be influenced by the distance between active sites.[3,50] Thus, their maximum population was detected as the contact time increased (from 24 to 72 h). Cells adhere to hydrogels that do not encourage binding; however, they frequently have a spherical shape or less stretching morphology and finally die as shown as red and green, presenting alive cells, as shown in Figure 6a. They lack actin stress fibers and exhibit reduced cell survival and proliferation (Figure 6a), as exhibited by GBG-1. The increased cell adherence was observed, as these are the fixed SEM images of the cell cultured over the hydrogel's films, as shown in Figure 6b. The red arrows indicate the cellular adherence; it was also found that increased cellular contact time (from 24 to 72 h) also increased the cellular populations over the hydrogel films. Hydrogels without binding sites may allow for cell adhesion by creating an extracellular matrix by adherent cells. Hence, the increased GO amount caused well-cell adherence that led to cell viability and proliferation due to the increasing multifunctional behavior of hydrogels.

5. CONCLUSIONS

The GO-*f*-BC was synthesized via the hydrothermal method using different amount of GO to optimize and determine the role of graphene oxide. The composite hydrogels were fabricated from GO-*f*-BC and gelatin by crosslinking with TEOS. These hydrogels are multifunctional biomaterials and have improved properties such as antimicrobial, biodegradability, biocompatibility, and bioactivities. FTIR confirmed the structural properties, functional group identification, and help to understand the physicochemical interactions. The different surface morphology and surface roughness were confirmed by SEM and AFM. The wetting properties was shifted from high hydrophilicity to low hydrophilicity with an increased GO amount, but increased swelling and biodegradation were observed from GBG-1 to GBG-4. GBG-4 has presented the maximum antibacterial activity against Gram (positive and negative) bacterial strains. All hydrogels were found to be hemocompatible with different concentrations of hydrogels against fresh blood. The hydrogel sample GBG-4 has exhibited enhanced cell viability and proliferation with mature cell morphology and improved cell adherence, among all other hydrogel formulations. Hence, these hydrogels might be promising and potential wound dressings for skin tissue engineering.

AUTHOR INFORMATION

Corresponding Authors

Rozita Hassan − *Orthodontic Unit, School of Dental Science, Universiti Sains Malaysia, Kubang Kerian, Kelantan 16150, Malaysia*; Email: rozitakb@usm.my

T. Joseph Sahaya Anand − *Sustainable and Responsive Manufacturing Group, Faculty of Mechanical and Manufacturing Engineering Technology, Universiti Teknikal Malaysia Melaka, Melaka 76100 Malacca, Malaysia*; Email: anand@utem.edu.my

Anwarul Hasan − *Biomedical Research Center and Department of Mechanical and Industrial Engineering, Qatar University, Doha 2713, Qatar*; orcid.org/0000-0001-8380-2233; Email: ahasan@qu.edu.qa

Authors

Muhammad Umar Aslam Khan − *Biomedical Research Center and Department of Mechanical and Industrial Engineering, Qatar University, Doha 2713, Qatar*; orcid.org/0000-0001-8105-2651

Goran M. Stojanović − *Faculty of Technical Sciences, University of Novi Sad, 21000 Novi Sad, Serbia*; orcid.org/0000-0003-2098-189X

Maryam Al-Ejji − *Center for Advanced Materials, Qatar University, Doha 2713, Qatar*

Complete contact information is available at: https://pubs.acs.org/10.1021/acsomega.2c07279

Notes

The authors declare no competing financial interest.

We thank the Central Lab Unit (CLU) and Centre for Advanced Materials (CAM) at Qatar University (QU) for their help with the SEM imaging.

Conceptualization, M.U.A.K.; data curation, M.U.A.K. and T.J.S.A.; formal analysis, M.U.A.K. and M.A.-E.; funding acquisition, M.U.A.K., R.H., and G.M.S.; investigation, G.M.S., T.J.S.A., and A.H.; methodology, M.U.A.K., A.H., and G.M.S.; project administration, M.U.A.K. and R.H.; resources, M.U.A.K., A.H., and M.A.-E.; software, M.U.A.K.; supervision, A.H., G.M.S., and R.H.; validation, A.H., R.H., and T.J.S.A.; visualization, M.U.A.K.; writing (original draft), M.U.A.K.; writing (review and editing), M.U.A.K. and G.M.S.

ACKNOWLEDGMENTS

We are grateful to the European Union's Horizon to support the research project. This project has received funding from the European Union's Horizon 2020 research and innovation program under grant agreement no. 951747 and acknowledge the NPRP award [NPRP 12S -0310-190276] from the Qatar National Research Fund (a member of The Qatar Foundation). The statements made herein are solely the responsibility of the authors.

REFERENCES

(1) Khan, M. U. A.; Razaq, S. I. A.; Mehboob, H.; Rehman, S.; Al-Arjan, W. S.; Amin, R. Antibacterial and hemocompatible pH-responsive hydrogel for skin wound healing application: In vitro drug release. *Polymer* **2021**, *13*, 3703.

(2) Zimoch, J.; Zielinska, D.; Michalak-Micka, K.; Rütsche, D.; Böni, R.; Biedermann, T.; Klar, A. S. Bio-engineering a prevascularized

https://doi.org/10.1021/acsomega.2c07279
ACS Omega 2023, 8, 15909−15919

human tri-layered skin substitute containing a hypodermis. *Acta Biomater.* **2021**, *134*, 215−227.
(3) Khan, M. U. A.; Haider, S.; Raza, M. A.; Shah, S. A.; Abd Razak, S. I.; Kadir, M. R. A.; Subhan, F.; Haider, A. Smart and pH-sensitive rGO/Arabinoxylan/chitosan composite for wound dressing: In-vitro drug delivery, antibacterial activity, and biological activities. *Int. J. Biol. Macromol.* **2021**, *192*, 820−831.
(4) Schlottmann, F.; Bucan, V.; Vogt, P. M.; Krezdorn, N. A short history of skin grafting in burns: from the gold standard of autologous skin grafting to the possibilities of allogeneic skin grafting with immunomodulatory approaches. *Medicina* **2021**, *57*, 225.
(5) Khan, M. U. A.; Abd Razak, S. I.; Haider, S.; Mannan, H. A.; Hussain, J.; Hasan, A. Sodium alginate-F-GO/sodium alginate composite hydrogels for tissue regeneration and antitumor applications. *Int. J. Biol. Macromol.* **2022**, 475.
(6) Correia Carreira, S.; Begum, R.; Perriman, A. W. 3D bioprinting: the emergence of programmable biodesign. *Adv. Healthcare Mater.* **2020**, *9*, 1900554.
(7) Nazir, S.; Khan, M. U. A.; Al-Arjan, W. S.; Abd Razak, S. I.; Javed, A.; Kadir, M. R. A. Nanocomposite hydrogels for melanoma skin cancer care and treatment: In-vitro drug delivery, drug release kinetics and anti-cancer activities. *Arabian J. Chem.* **2021**, *14*, No. 103120.
(8) Khan, M. U. A.; Haider, A.; Abd Razak, S. I.; Kadir, M. R. A.; Haider, S.; Shah, S. A.; Hasan, A.; Khan, R.; Khan, S.; Shakir, I. Arabinoxylan/graphene-oxide/nHAp-NPs/PVA bionano composite scaffolds for fractured bone healing. *J. Tissue Eng. Regener. Med.* **2021**, *15*, 322−335.
(9) Aslam Khan, M. U.; Al-Arjan, W. S.; Binkadem, M. S.; Mehboob, H.; Haider, A.; Raza, M. A.; Abd Razak, S. I.; Hasan, A.; Amin, R. Development of Biopolymeric Hybrid Scaffold-Based on AAc/GO/nHAp/TiO2 Nanocomposite for Bone Tissue Engineering: In-Vitro Analysis. *Nanomaterials* **2021**, *11*, 1319.
(10) Liu, B.; Huang, W.; Yang, G.; An, Y.; Yin, Y.; Wang, N.; Jiang, B. Preparation of gelatin/poly (γ-glutamic acid) hydrogels with stimulated response by hot-pressing preassembly and radiation crosslinking. *Mater. Sci. Eng., C* **2020**, *116*, No. 111259.
(11) Khan, M. U. A.; Iqbal, I.; Ansari, M. N. M.; Razak, S. I. A.; Raza, M. A.; Sajjad, A.; Jabeen, F.; Riduan Mohamad, M.; Jusoh, N. Development of antibacterial, degradable and ph-responsive chitosan/guar gum/polyvinyl alcohol blended hydrogels for wound dressing. *Molecules* **2021**, *26*, 5937.
(12) Zerankeshi, M. M.; Bakhshi, R.; Alizadeh, R. Polymer/metal composite 3D porous bone tissue engineering scaffolds fabricated by additive manufacturing techniques: A review. *Bioprinting* **2022**, No. e00191.
(13) Hu, X.; Xia, Z.; Cai, K. Recent advances of 3D hydrogel culture systems for mesenchymal stem cell-based therapy and cell behavior regulation. *J. Mater. Chem. B* **2022**, 1486.
(14) Khan, M. U. A.; Yaqoob, Z.; Ansari, M. N. M.; Razak, S. I. A.; Raza, M. A.; Sajjad, A.; Haider, S.; Busra, F. M. Chitosan/Poly Vinyl Alcohol/Graphene Oxide Based pH-Responsive Composite Hydrogel Films: Drug Release, Antimicrobial and Cell Viability Studies. *Polymer* **2021**, *13*, 3124.
(15) Albuquerque, P. B. S.; de Oliveira, W. F.; dos Santos Silva, P. M.; dos Santos Correia, M. T.; Kennedy, J. F.; Coelho, L. C. B. B. Epiphanies of well-known and newly discovered macromolecular carbohydrates−a review. *Int. J. Biol. Macromol.* **2020**, *156*, 51−66.
(16) Raghav, N.; Sharma, M. R.; Kennedy, J. F. Nanocellulose: A mini-review on types and use in drug delivery systems. *Carbohydr. Polym. Technol. Appl.* **2021**, *2*, No. 100031.
(17) Khan, M. U. A.; Rizwan, M.; Abd Razak, S. I.; Hassan, A.; Rasheed, T.; Bilal, M. Electroactive polymeric nanocomposite BC-g-(Fe3O4/GO) materials for bone tissue engineering: In-vitro evaluations. *J. Biomater. Sci., Polym. Ed.* **2022**, 1349−1368.
(18) Haghighatpanah, N.; Omar-Aziz, M.; Gharaghani, M.; Khodaiyan, F.; Hosseini, S. S.; Kennedy, J. F. Effect of mung bean protein isolate/pullulan films containing marjoram (Origanum majorana L.) essential oil on chemical and microbial properties of minced beef meat. *Int. J. Biol. Macromol.* **2022**, 318.
(19) Singh, R. S.; Kaur, N.; Hassan, M.; Kennedy, J. F. Pullulan in biomedical research and development-A review. *Int. J. Biol. Macromol.* **2021**, *166*, 694−706.
(20) Aga, M. B.; Dar, A. H.; Nayik, G. A.; Panesar, P. S.; Allai, F.; Khan, S. A.; Shams, R.; Kennedy, J. F.; Altaf, A. Recent insights into carrageenan-based bio-nanocomposite polymers in food applications: A review. *Int. J. Biol. Macromol.* **2021**, *192*, 197−209.
(21) Selvamani, P. S.; Vijaya, J. J.; Kennedy, L. J.; Saravanakumar, B.; Bououdina, M.; Rajabathar, J. R. Design of copper (II) oxide nanoflakes decorated with molybdenum disulfide@ reduced graphene oxide composite as an electrode for high performance supercapacitor. *Synth. Met.* **2021**, *278*, No. 116843.
(22) Abba, M.; Ibrahim, Z.; Chong, C. S.; Zawawi, N. A.; Kadir, M. R. A.; Yusof, A. H. M.; Razak, S. I. A. Transdermal delivery of crocin using bacterial nanocellulose membrane. *Fibers Polym.* **2019**, *20*, 2025−2031.
(23) Repetto, G.; Del Peso, A.; Zurita, J. L. Neutral red uptake assay for the estimation of cell viability/cytotoxicity. *Nat. Protoc.* **2008**, *3*, 1125−1131.
(24) Khan, M. U. A.; Haider, S.; Haider, A.; Abd Razak, S. I.; Kadir, M. R. A.; Shah, S. A.; Javed, A.; Shakir, I.; Al-Zahrani, A. A. Development of porous, antibacterial and biocompatible GO/n-HAp/bacterial cellulose/β-glucan biocomposite scaffold for bone tissue engineering. *Arabian J. Chem.* **2021**, *14*, No. 102924.
(25) Treesuppharat, W.; Rojanapanthu, P.; Siangsanoh, C.; Manuspiya, H.; Ummartyotin, S. Synthesis and characterization of bacterial cellulose and gelatin-based hydrogel composites for drug-delivery systems. *Biotechnol. Rep.* **2017**, *15*, 84−91.
(26) Song, Q.; Miao, C.; Sai, H.; Gu, J.; Wang, M.; Jiang, P.; Wang, Y.; Fu, R.; Wang, Y. Silica-Bacterial Cellulose Composite Aerogel Fibers with Excellent Mechanical Properties from Sodium Silicate Precursor. *Gels* **2022**, *8*, 17.
(27) Zhu, S.; Dai, Q.; Yao, L.; Wang, Z.; He, Z.; Li, M.; Wang, H.; Li, Q.; Gao, H.; Cao, X. Engineered multifunctional nanocomposite hydrogel dressing to promote vascularization and anti-inflammation by sustained releasing of Mg2+ for diabetic wounds. *Composites, Part B* **2022**, *231*, No. 109569.
(28) Khan, M. U. A.; Razak, S. I. A.; Hasan, A.; Qureshi, S.; Stojanovic, G.; Khan, M. U. A. U. Multifunctional composite hydrogels for wound healing application: In-vitro and in-vivo evaluations. *Front. Bioeng. Biotechnol.* , 536.
(29) Dev, A.; Mohanbhai, S. J.; Kushwaha, A. C.; Sood, A.; Sardoiwala, M. N.; Choudhury, S. R.; Karmakar, S. κ-carrageenan-C-phycocyanin based smart injectable hydrogels for accelerated wound recovery and real-time monitoring. *Acta Biomater.* **2020**, *109*, 121−131.
(30) Vialar, P.; Merzeau, P.; Barthel, E.; Giasson, S.; Drummond, C. Interaction between compliant surfaces: how soft surfaces can reduce friction. *Langmuir* **2019**, *35*, 15723−15728.
(31) Mao, L.; Wang, L.; Zhang, M.; Ullah, M. W.; Liu, L.; Zhao, W.; Li, Y.; Ahmed, A. A. Q.; Cheng, H.; Shi, Z.; Yang, G. In Situ Synthesized Selenium Nanoparticles-Decorated Bacterial Cellulose/Gelatin Hydrogel with Enhanced Antibacterial, Antioxidant, and Anti-Inflammatory Capabilities for Facilitating Skin Wound Healing. *Adv. Healthcare Mater.* **2021**, *10*, 2100402.
(32) Unal, S.; Arslan, S.; Yilmaz, B. K.; Oktar, F. N.; Sengil, A. Z.; Gunduz, O. Production and characterization of bacterial cellulose scaffold and its modification with hyaluronic acid and gelatin for glioblastoma cell culture. *Cellulose* **2021**, *28*, 117−132.
(33) Jiang, H.; Duan, L.; Ren, X.; Gao, G. Hydrophobic association hydrogels with excellent mechanical and self-healing properties. *Eur. Polym. J.* **2019**, *112*, 660−669.
(34) Ngo, C. V.; Chun, D. M. Effect of Heat Treatment Temperature on the Wettability Transition from Hydrophilic to Superhydrophobic on Laser-Ablated Metallic Surfaces. *Adv. Eng. Mater.* **2018**, *20*, 1701086.

https://doi.org/10.1021/acsomega.2c07279
ACS Omega 2023, 8, 15909−15919

(35) Khan, S.; Anwar, N. Gelatin/carboxymethyl cellulose based stimuli-responsive hydrogels for controlled delivery of 5-fluorouracil, development, in vitro characterization, in vivo safety and bioavailability evaluation. *Carbohydr. Polym.* **2021**, *257*, No. 117617.
(36) Borges-Vilches, J.; Figueroa, T.; Guajardo, S.; Aguayo, C.; Fernández, K. Improved hemocompatibility for gelatin-graphene oxide composite aerogels reinforced with proanthocyanidins for wound dressing applications. *Colloids Surf., B* **2021**, *206*, No. 111941.
(37) Yan, X.; Yang, J.; Chen, F.; Zhu, L.; Tang, Z.; Qin, G.; Chen, Q.; Chen, G. Mechanical properties of gelatin/polyacrylamide/graphene oxide nanocomposite double-network hydrogels. *Compos. Sci. Technol.* **2018**, *163*, 81−88.
(38) Hasturk, O.; Jordan, K. E.; Choi, J.; Kaplan, D. L. Enzymatically crosslinked silk and silk-gelatin hydrogels with tunable gelation kinetics, mechanical properties and bioactivity for cell culture and encapsulation. *Biomaterials* **2020**, *232*, No. 119720.
(39) Bhagat, A. A. S.; Hou, H. W.; Li, L. D.; Lim, C. T.; Han, J. Pinched flow coupled shear-modulated inertial microfluidics for high-throughput rare blood cell separation. *Lab Chip* **2011**, *11*, 1870−1878.
(40) Dacrory, S.; Hashem, A. H.; Hasanin, M. Synthesis of cellulose based amino acid functionalized nano-biocomplex: characterization, antifungal activity, molecular docking and hemocompatibility. *Environ. Nanotechnol., Monit. Manage.* **2021**, *15*, No. 100453.
(41) Zhou, J.; Zhang, S.; Song, X.; Wei, R.; Zhang, X.; Zhao, W.; Zhao, C. Three-dimensional graphene oxide skeleton guided poly (acrylic acid) composite hydrogel particles with hierarchical pore structure for hemoperfusion. *ACS Biomater. Sci. Eng.* **2019**, *5*, 3987−4001.
(42) Sundaram, M. N.; Mony, U.; Varma, P. K.; Rangasamy, J. Vasoconstrictor and coagulation activator entrapped chitosan based composite hydrogel for rapid bleeding control. *Carbohydr. Polym.* **2021**, *258*, No. 117634.
(43) Zhan, Y.; Zeng, W.; Jiang, G.; Wang, Q.; Shi, X.; Zhou, Z.; Deng, H.; Du, Y., Construction of lysozyme exfoliated rectorite-based electrospun nanofibrous membranes for bacterial inhibition. *J. Appl. Polym. Sci.* 2015, *132* (), DOI: 10.1002/app.41496.
(44) Obuobi, S.; Tay, H. K.-L.; Tram, N. D. T.; Selvarajan, V.; Khara, J. S.; Wang, Y.; Ee, P. L. R. Facile and efficient encapsulation of antimicrobial peptides via crosslinked DNA nanostructures and their application in wound therapy. *J. Controlled Release* **2019**, *313*, 120−130.
(45) Zhang, X.; Qin, M.; Xu, M.; Miao, F.; Merzougui, C.; Zhang, X.; Wei, Y.; Chen, W.; Huang, D. The fabrication of antibacterial hydrogels for wound healing. *Eur. Polym. J.* **2021**, *146*, No. 110268.
(46) Khan, M. U. A.; Raza, M. A.; Razak, S. I. A.; Abdul Kadir, M. R.; Haider, A.; Shah, S. A.; Mohd Yusof, A. H.; Haider, S.; Shakir, I.; Aftab, S. Novel functional antimicrobial and biocompatible arabinoxylan/guar gum hydrogel for skin wound dressing applications. *J. Tissue Eng. Regener. Med.* **2020**, *14*, 1488−1501.
(47) Khan, M. U. A.; Raza, M. A.; Mehboob, H.; Kadir, M. R. A.; Abd Razak, S. I.; Shah, S. A.; Iqbal, M. Z.; Amin, R. Development and in vitro evaluation of κ-carrageenan based polymeric hybrid nanocomposite scaffolds for bone tissue engineering. *RSC Adv.* **2020**, *10*, 40529−40542.
(48) Khan, M. U. A.; Haider, S.; Shah, S. A.; Abd Razak, S. I.; Hassan, S. A.; Kadir, M. R. A.; Haider, A. Arabinoxylan-co-AA/HAp/TiO2 nanocomposite scaffold a potential material for bone tissue engineering: An in vitro study. *Int. J. Biol. Macromol.* **2020**, *151*, 584−594.
(49) Ahearne, M. Introduction to cell−hydrogel mechanosensing. *Interface Focus* **2014**, *4*, 20130038.
(50) Khan, M. U. A.; Abd Razak, S. I.; Hassan, A.; Qureshi, S.; Stojanović, G. M., Multifunctional Arabinoxylan-functionalized-Graphene Oxide Based Composite Hydrogel for Skin Tissue Engineering. *Front. Bioeng. Biotechnol.* 2022, *10*, DOI: 10.3389/fbioe.2022.865059.

NOTE ADDED AFTER ASAP PUBLICATION

This paper was originally published ASAP on March 27, 2023. A minor change was made to the title, and the Abstract was replaced. The corrected version reposted on April 25, 2023.

https://doi.org/10.1021/acsomega.2c07279
ACS Omega 2023, 8, 15909−15919